Spectroscopic and Kinetic Study of the Gas-Phase CH_3I-Cl and C_2H_5I-Cl Adducts†

V. Dookwah-Roberts,‡ J. M. Nicovich,§ and P. H. Wine*,‡,§

School of Earth and Atmospheric Sciences, School of Chemistry and Biochemistry, Georgia Institute of Technology, Atlanta, Georgia 30332

Received: January 11, 2008; Revised Manuscript Received: February 13, 2008

Time-resolved UV–visible absorption spectroscopy has been coupled with UV laser flash photolysis of Cl_2/RI/N_2/X mixtures (R = CH_3 or C_2H_5; X = O_2, NO, or NO_2) to generate the RI−Cl radical adducts in the gas phase and study the spectroscopy and reaction kinetics of these species. Both adducts were found to absorb strongly over the wavelength range 310–500 nm. The spectra were very similar in wavelength dependence with $\lambda_{max} \approx 315$ nm for both adducts and $\sigma_{max} = (3.5 \pm 1.2) \times 10^{-17}$ and $(2.7 \pm 1.0) \times 10^{-17}$ cm^2 molecule^{-1} (base e) for CH_3I-Cl and C_2H_5I-Cl, respectively (uncertainties are estimates of accuracy at the 95% confidence level). Two weaker bands with $\lambda_{max} \sim 350$ and 420 nm were also observed. Over the wavelength range 405–500 nm, where adduct spectra are reported both in the literature and in this study, the absorption cross sections obtained in this study are a factor of ~4 lower than those reported previously [Enami et al. *J. Phys. Chem. A* **2005**, *109*, 1587 and 6066]. Reactions of RI−Cl with O_2 were not observed, and our data suggest that upper limit rate coefficients for these reactions at 250 K are 1.0×10^{-17} cm^3 molecule^{-1} s^{-1} for R = CH_3 and 2.5×10^{-17} cm^3 molecule^{-1} s^{-1} for R = C_2H_5. Their lack of reactivity with O_2 suggests that RI−Cl adducts are unlikely to play a significant role in atmospheric chemistry. Possible reactions of RI−Cl with RI could not be confirmed or ruled out, although our data suggest that upper limit rate coefficients for these reactions at 250 K are 3×10^{-13} cm^3 molecule^{-1} s^{-1} for R = CH_3 and 5×10^{-13} cm^3 molecule^{-1} s^{-1} for R = C_2H_5. Rate coefficients for CH_3I-Cl reactions with CH_3I-Cl (k_9), NO (k_{22}), and NO_2 (k_{24}), and C_2H_5I-Cl reactions with C_2H_5I-Cl (k_{14}), NO (k_{23}), and NO_2 (k_{25}) were measured at 250 K. In units of 10^{-11} cm^3 molecule^{-1} s^{-1}, the rate coefficients were found to be $2k_9 = 35 \pm 12$, $k_{22} = 1.8 \pm 0.4$, $k_{24} = 3.3 \pm 0.6$, $2k_{14} = 40 \pm 16$, $k_{23} = 1.8 \pm 0.3$, and $k_{25} = 4.0 \pm 0.9$, where the uncertainties are estimates of accuracy at the 95% confidence level.

Introduction

Iodine-containing organic compounds, such as CH_3I, CH_2I_2, CH_2ICl, C_2H_5I and larger alkyl iodides, are produced by metabolic processes in macroalgae and phytoplankton in the ocean and are subsequently emitted into the atmosphere.[1–12] Unlike other halocarbons, alkyl iodides are photochemically active in the lower atmosphere; that is, they absorb solar radiation in the near-ultraviolet region of the spectrum and have high quantum yields for photolytic release of an iodine atom. Reactions of alkyl iodides with OH radicals and Cl atoms have been studied experimentally and theoretically, since these reactions also contribute to alkyl iodide degradation, ultimately yielding iodine atoms that participate in HO_2/OH and NO_2/NO cycling, thereby influencing the oxidizing capacity of the troposphere.[6,13–16] Iodine-containing molecules, especially OIO, have been implicated in aerosol formation in coastal areas.[17–19] Iodine chemistry may also play a role in tropospheric and lower stratospheric ozone depletion.[16,20]

The first indication that Cl reactions with iodoalkanes may involve a complex mechanism came from product angular distributions observed in molecular beam studies by Hoffmann et al.[21,22] Evidence for production of a thermalized CH_3I-Cl adduct was first reported by Ayhens et al.[23] These investigators followed Cl kinetics over a wide range of temperature and pressure and demonstrated that both addition and H-abstraction pathways were operative:

$$Cl + CH_3I \rightarrow CH_2I + HCl \quad (1a)$$

$$Cl + CH_3I + M \leftrightarrow CH_3I-Cl + M \quad (1b, -1b)$$

At 364 K ≤ T ≤ 694 K, the rate coefficient, $k_{1a} = 5.4 \times 10^{-11} \exp(-1250/T)$ cm^3 molecule^{-1} s^{-1} was reported, and a significant kinetic isotopic effect was observed at 373 K ($k_1^H/k_1^D = 4.3$), providing evidence that H-abstraction was dominant under these conditions. At $T \leq 250$ K, reaction occurred via formation of a stable adduct with a reported rate coefficient $k_{1b} \approx 2 \times 10^{-11}$ cm^3 molecule^{-1} s^{-1} at $P = 500$ Torr N_2. Rate coefficients for reactions 1b and −1b were determined as a function of temperature and pressure over the ranges 263–309 K and 25–500 Torr N_2, respectively. From a combination of second- and third-law analyses, Ayhens et al. deduced a 0 K adduct bond dissociation energy of 52.2 ± 3.3 kJ mol^{-1}, in reasonable agreement with their theoretical value of 59.3 kJ mol^{-1} obtained using density functional theory (DFT) at the B3LYP/ECP level and also in good agreement with a theoretical value of 50.7 kJ mol^{-1} reported by Lazarou et al.[24] based on calculations at the MP2/3–21++G(2d,2p) level of theory.

Several additional studies of the Cl + CH_3I reaction are reported in the literature. Kambanis et al.[25] conducted low-pressure studies ($P \sim 2$ mTorr) over the temperature range 273–363 K and reported the Arrhenius expression $k_1 = 1.3 \times 10^{-11} \exp(-689/T)$ cm^3 molecule^{-1} s^{-1}.[25] Evidence for a kinetic isotope effect was not observed ($k_H/k_D = 1.09 \pm 0.04$), leading

† Part of the "Stephen R. Leone Festschrift".
* Corresponding author.
‡ School of Earth and Atmospheric Sciences.
§ School of Chemistry and Biochemistry.

10.1021/jp800270r CCC: $40.75
Published on Web 06/03/2008

these investigators to conclude that reaction 1 proceeds via a weakly bound CH_3I-Cl adduct.[25] Product studies of reaction 1 have been reported by Goliff and Rowland,[26] who report a 9% yield of CH_3Cl at 295 K and pressures in the range of 760 – 4000 Torr $CClF_3$, as well as by Bilde and Wallington,[27] who report an upper limit CH_3Cl yield of 20% at $T = 295$ K and $P = 1$ Torr N_2 and a 50% increase in reactivity upon raising the pressure to 700 Torr N_2, air, or O_2, suggesting the occurrence of adduct loss processes other than reaction −1b:

$$CH_3I-Cl + M \rightarrow M + \text{products other than } CH_3I + Cl \quad (2)$$

$$CH_3I + CH_3I-Cl \rightarrow CH_3Cl + \text{other products} \quad (3)$$

In contrast to the findings of Kambanis et al., Bilde and Wallington observed a large kinetic isotopic effect ($k_H/k_D = 6$ at 295 K and 1 Torr N_2), thereby concluding that reaction 1a is the dominant channel under their low-pressure experimental conditions; they report a rate coefficient of $k_{1a}(295\ K) = 9.0 \times 10^{-13}$ cm^3 molecule^{-1} s^{-1}, in good agreement with the rate coefficient obtained by extrapolation of the high-temperature results of Ayhens et al.[23] to 295 K, assuming Arrhenius behavior. Cotter et al. report a rate coefficient of $k_1 = 1.5 \times 10^{-12}$ cm^3 molecule^{-1} s^{-1} at 298 K and over the pressure range 1.5–12 Torr He[28] which, under their experimental conditions, they attribute primarily to pathway 1a. Cotter et al. also have conducted end product analysis studies of reactions 1 and 4 in air at atmospheric pressure and room temperature[29] and conclude that both reactions proceed via two channels: one yielding HCl and an iodinated alkyl radical, consistent with reaction 1a (for CH_3I) or reactions 4a and 4b (for C_2H_5I), and the other yielding I atoms, an alkyl chloride, and a carbonyl species, consistent with reactions 1b, −1b, and 3 (for CH_3I) or reactions 4c, –4c, and 5 (for C_2H_5I):

$$Cl + CH_3CH_2I \rightarrow CH_3CHI + HCl \quad (4a)$$

$$\rightarrow CH_2CH_2I + HCl \quad (4b)$$

$$Cl + CH_3CH_2I + M \leftrightarrow CH_3CH_2I-Cl + M \quad (4c)$$

$$CH_3CH_2I + CH_3CH_2I-Cl \rightarrow CH_3CH_2Cl + \text{other products} \quad (5)$$

A combined laser flash photolysis (LFP), competitive kinetics, end product analysis, and theoretical study of reaction 4 has been reported by Orlando et al.[30] These investigators report Arrhenius expressions for Cl reactions with C_2H_5I and C_2D_5I applicable over the temperature range 334–434 K, where H-transfer pathways are found to dominate. In units of cm^3 molecule^{-1} s^{-1}, the reported Arrhenius expressions are $k_4^H = 6.5 \times 10^{-11} \exp(-428/T)$ and $k_4^D = 2.2 \times 10^{-11} \exp(-317/T)$. In addition, Orlando et al. report branching ratios for abstraction pathways at 298 K of 63% and 37% for channels 4a and 4b, respectively.[30] Equilibration kinetics for reactions 4c and –4c were investigated at subambient temperatures, yielding a 0 K bond energy for CD_3CD_2I-Cl of 57 ± 10 kJ/mol; published theoretical values for the CH_3CH_2I-Cl bond strength[30,31] are consistent with the experimental value. Using product studies in conjunction with competitive kinetics techniques, Orlando et al. estimate that k_5 (298 K) ~ (2–5) × 10^{-13} cm^3 molecule^{-1} s^{-1}.

By coupling laser flash photolysis with cavity ring down spectroscopy, Enami et al.[31,32] have directly observed the adducts CH_3I-Cl and C_2H_5I-Cl for the first time. Their studies, which were carried out at $T = 250$ K and $P = 25$–125 Torr of N_2, provide wavelength-dependent absorption cross sections at $\lambda \geq 405$ nm, a wavelength range that appears to represent only the red tail of the absorption spectra. Recently, laser-induced fluorescence from CH_3I-Cl excited in the near UV spectral region has been reported by Gravestock et al. (this issue).[33]

In this paper, we report the results of an experimental study of the gas phase Cl + CH_3I and Cl + C_2H_5I reactions that couples LFP production of Cl with product detection by time-resolved UV–visible absorption spectroscopy (TRUVVAS). The gas phase absorption spectra of the CH_3I-Cl and C_2H_5I-Cl adducts at wavelengths shorter than 405 nm are reported for the first time, and wavelength-dependent absorption cross sections that are in rather poor agreement with literature values[31,32] over the overlapping wavelength regime of the studies (405–500 nm) are reported. In addition, the TRUVVAS technique is used as a probe to investigate the kinetics of adduct radical–radical reactions and adduct reactions with RI, O_2, NO, and NO_2. Although our findings suggest that CH_3I-Cl and C_2H_5I-Cl are of only minor importance in atmospheric chemistry, the results reported in this study are useful for developing an understanding of the kinetics and spectroscopy of gas-phase adducts of radicals with iodine compounds and, more generally, radical-molecule adducts that involve the formation of 2-center−3-electron (2c−3e) bonds; a number of such adducts do play important roles in atmospheric chemistry.

Experimental Technique

The LFP-TRUVVAS apparatus used in this study is nearly identical to those we have employed in previous spectroscopic and kinetic studies of adducts formed from reactions of atomic chlorine with CH_3SCH_3,[34] CS_2,[35] and $CH_3S(O)CH_3$.[36] A schematic diagram of the apparatus as well as a description of its operation are presented elsewhere.[35] Experimental details that are specific to this study are discussed below.

All experiments were carried out at temperatures in the range 250–261 K. The reaction cell and premixing cell were surrounded by an insulated Pyrex jacket through which an ethanol/methanol mixture was flowed from a temperature-controlled reservoir, enabling the cell temperature to be controlled. The temperatures of the gas mixture at the two exits from the reaction cell were measured with thermocouples. The temperature gradient between the ends of the cell was <2 °C, and the average of the temperatures measured at the two ends was taken to be the cell temperature. Dry nitrogen gas was sprayed onto the exterior of the quartz cell windows to prevent condensation of water vapor when the cell was cooled. Monochromator entrance and exit slits were set at 1.5 mm, providing a spectral resolution of 5.5 nm full width at half-maximum (fwhm).

For all kinetic measurements as well as for some spectroscopic studies at wavelengths longer than 350 nm, the RI−Cl adducts were generated by 308 nm laser flash photolysis of Cl_2 in the presence of RI (R = CH_3, C_2H_5). The absorption cross section for Cl_2 at 308 nm is 1.72×10^{-19} cm^2 molecule^{-1},[37] a typical photolysis fluence was ~20 mJ cm^{-2} pulse^{-1}, and the pulse duration was ~25 ns. For additional spectroscopic studies over the wavelength range 310–500 nm, RI−Cl adducts were generated by 248 nm laser flash photolysis of RI in the presence of Cl_2. Absorption cross sections for CH_3I and C_2H_5I at 248 nm are 8.4×10^{-19} and 8.7×10^{-19} cm^2 molecule^{-1}, respectively.[37] A typical photolysis fluence was 28 mJ cm^{-2} pulse^{-1}, and, as was the case for 308 nm photolysis, the pulse duration was ~25 ns.

All experiments were carried out under "slow flow" conditions; that is, the linear flow rate of the reaction mixture through

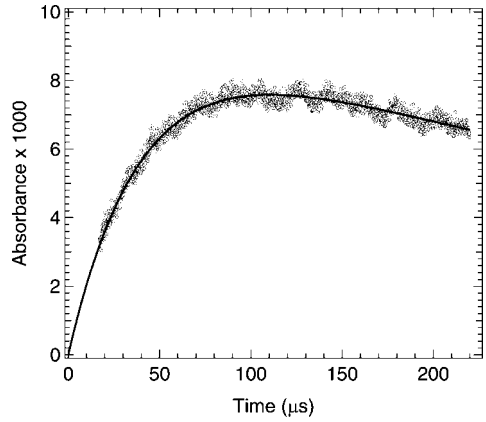

Figure 1. Typical absorbance (base e) temporal profile observed following laser flash photolysis of $RI/Cl_2/N_2$ mixtures at 308 nm. Experimental conditions: $T = 258$ K; $P = 263$ Torr; $R = C_2H_5$; monitoring wavelength = 365 nm; concentrations in units of 10^{14} molecules cm^{-3} are $[Cl_2] = 13.7$, $[C_2H_5I] = 2.04$, and $[Cl]_0 \approx 0.07$. The solid line is obtained from a nonlinear least-squares fit of the data to the sum of an exponential rise and an exponential decay. Best fit appearance (k_a) and disappearance (k_d) rate coefficients in units of s^{-1} are $k_a = 23810$ and $k_d = 2120$.

the reaction cell (typically 10 cm s^{-1}) was fast enough to replenish the entire volume of the reaction cell between photolysis laser pulses (laser repetition rate was 0.1 Hz, and the cell length was 100 cm) but slow enough that kinetic observations could be analyzed assuming static conditions.

Concentrations of both RI and Cl_2 were measured in situ in the slow flow system by UV photometry as well as by mass flow measurements. The in situ photometry measurements of CH_3I and C_2H_5I employed 254 nm as the monitoring wavelength (Hg penray lamp light source). The cross sections used to convert 254 nm absorbances to concentrations were 1.16×10^{-18} and 1.28×10^{-18} cm^2 $molecule^{-1}$ for CH_3I and C_2H_5I, respectively.[37] The in situ photometry measurements of Cl_2 employed 326 nm as the monitoring wavelength (Cd penray lamp light source). The cross section used to convert the 326 nm absorbance to concentration was 2.48×10^{-19} cm^2 $molecule^{-1}$.[37]

In the kinetics experiments, the concentrations of NO and NO_2 were determined from mass flow measurements of NO_2/N_2 or $NO_2/N_2/O_2$ mixtures combined with photometric measurements of the NO_2 mole fraction in the $NO_2/N_2/O_2$ mixtures. First, NO was transferred into a 12 L Pyrex bulb and diluted with N_2. Pressure measurements provided an initial estimate of the fraction of NO in the NO/N_2 mixture. Upon conclusion of a set of $RI-Cl + NO$ experiments, the NO/N_2 mixture was quantitatively diluted with enough O_2 to convert all NO to NO_2. After allowing several hours for conversion of NO to NO_2, the NO_2 was measured by UV photometry at 366 nm using a Hg lamp as the light source; the absorption cross section used to convert the measured absorbance to an NO_2 concentration was 6.05×10^{-19} cm^2 $molecule^{-1}$.[38] The NO concentration was determined quantitatively from the measured NO_2 concentration and the known O_2 dilution factor, whereas the resulting mixture was used for a set of $RI-Cl + NO_2$ experiments.

The pure gases used in this study were obtained from Air Products (O_2, N_2) and Spectra Gases (Cl_2, NO) and had the following stated minimum purities: N_2, 99.999%; O_2, 99.994%; Cl_2, 99.0%; and NO, 99.0%. The N_2 and O_2 were used as supplied. The Cl_2 and NO were degassed at 77 K prior to use. Iodomethane (Fisher Scientific) and iodoethane (Sigma-Aldrich) had stated minimum purities of 99.9% and 99%, respectively. The iodoalkanes were transferred under N_2 into vials fitted with high-vacuum stopcocks. After repeated degassing at 77 K, appropriate amounts were transferred into 12 L Pyrex bulbs and diluted with N_2.

Results and Discussion

When Cl_2 was photolyzed at 308 nm in the presence of RI, absorption of the UV–visible probe beam was observed throughout the 350−500 nm spectral region. Similarly, when RI was photolyzed at 248 nm in the presence of Cl_2, absorption of the UV–visible probe beam was observed throughout the 310−500 nm spectral region. In both cases, absorption was observed only when both RI and Cl_2 were present in the photolyzed gas mixture.

Identification of the Absorbing Species. Evidence verifying the identity of the absorbing species was obtained by measuring its appearance rate. Absorbance temporal profiles were recorded and analyzed using a nonlinear least-squares fit to eq I, which describes the time evolution of the intermediate in consecutive first-order reactions: [39]

$$A_t = [k_a/(k_d - k_a)]X[\exp(-k_a t) - \exp(-k_d t)] \qquad (I)$$

In the above equation, A_t is the absorbance at time t, k_a is the first-order absorbance appearance rate, k_d is the first-order absorbance decay rate, and X is the peak adduct absorbance that would be observed in the absence of a decay. A typical absorbance temporal profile is shown in Figure 1. In this set of experiments, absorbance disappearance resulted primarily from radical–radical reactions and was not a first-order process. The first-order absorbance disappearance rate, k_d, is thus a parametrized rate coefficient rather than the sum of actual loss processes that are quantitatively attributable to specific first order processes. However, because (i) the observed absorbance loss rates are slow compared to the rates of absorbance appearance and (ii) the data that were fit were limited to times when the fractional decay of absorbance was small, the parametrization of the absorbance disappearance as a first order process does not seriously impact the reliability of the analysis to determine the pseudo-first-order rate coefficient for absorbance appearance. As typified by the data shown in Figure 1, the quality of the double exponential fits is quite good. Pseudo-first-order appearance rate coefficients (k_a) were measured at 350 nm in 100 Torr N_2 buffer gas and at 365 nm in 260 Torr N_2 buffer gas for CH_3I-Cl and C_2H_5I-Cl, respectively. As shown in Figure 2, plots of k_a vs [RI] are linear over the range of RI concentrations employed. The linearity of the k_a vs [RI] plots up to the fastest appearance rates measured (~60 000 and 40 000 s^{-1} for $Cl + CH_3I$ and $Cl + C_2H_5I$, respectively) demonstrates that the rate-limiting step in production of the absorbing species is the $Cl + RI$ reaction under the conditions investigated. The slopes of the k_a-vs-[RI] plots yield the second order rate coefficients, $k_1 = (1.0 \pm 0.2) \times 10^{-11}$ cm^3 $molecule^{-1}$ s^{-1} at $T = 261$ K and $P = 100$ Torr N_2 and $k_4 = (1.1 \pm 0.1) \times 10^{-10}$ cm^3 $molecule^{-1}$ s^{-1} at $T = 258$ K and $P = 260$ Torr N_2, where $k_1 \equiv k_{1a} + k_{1b}$, $k_4 \equiv k_{4a} + k_{4b} + k_{4c}$, and the uncertainties are 2σ and represent precision only. The values for k_1 and k_4 evaluated from the absorbance appearance rates agree within experimental uncertainty with $Cl + RI$ rate coefficients obtained at the same temperatures and pressures by monitoring the decay of Cl using atomic resonance fluorescence spectroscopy.[23,30] The data in Figures 1 and 2 provide strong evidence that the species being observed are indeed the $RI-Cl$ adducts formed as primary products of the reactions of Cl with RI.

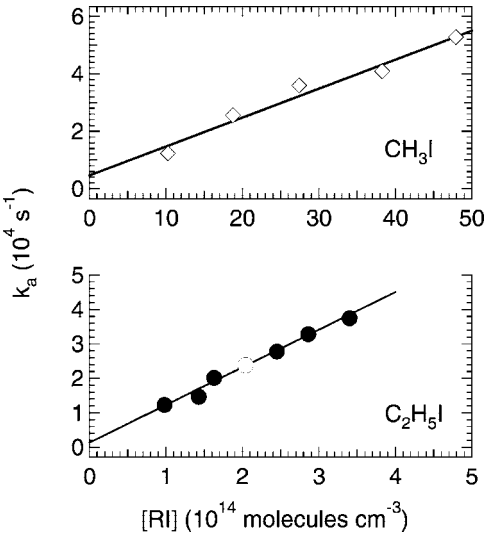

Figure 2. Plots of k_a versus $[CH_3I]$ for data obtained at $T = 261$ K and $P = 100$ Torr N_2 and k_a versus $[C_2H_5I]$ for data obtained at $T = 258$ K and $P = 263$ Torr N_2. The solid lines are obtained from linear least-squares analyses; their slopes give the following second-order rate coefficients in units of 10^{-11} cm^3 $molecule^{-1}$ s^{-1}: $k_1 = 1.01 \pm 0.21$ and $k_4 = 10.9 \pm 0.48$. The open C_2H_5I data point is the one obtained from the data shown in Figure 1.

Adduct Absorption Spectra. The absorption spectrum of CH_3I-Cl was measured at 300 Torr total pressure (N_2 bath gas) and 250 K using two different methods of Cl generation. The first method involved 308 nm photolysis of Cl_2:

$$Cl_2 + h\nu\ (308\ nm) \rightarrow 2Cl \quad (6)$$

$$CH_3I + Cl + M \rightarrow CH_3I-Cl + M \quad (6b)$$

The second method employed 248 nm photolysis of CH_3I:

$$CH_3I + h\nu\ (248\ nm) \rightarrow CH_3 + I \quad (7)$$

$$CH_3 + Cl_2 \rightarrow CH_3Cl + Cl \quad (8)$$

$$CH_3I + Cl + M \rightarrow CH_3I-Cl + M \quad (8b)$$

Using the first method, absorption measurements were made over the wavelength range 350–500 nm, whereas the second method facilitated absorption measurements over the wider wavelength range 310–500 nm. A reference wavelength of 350 nm was selected for the CH_3I-Cl spectral measurements. Absorption measurements were made at this reference wavelength after every 5 measurements at other wavelengths. This was done to account for systematic drifts in experimental parameters, such as laser power, $[Cl_2]$, optical alignment, etc., over time. Absorbance measurements at wavelengths other than 350 nm were normalized to the average of the "before" and "after" 350 nm absorbances. The adduct absorption cross section was carefully measured at 350 nm, and all cross sections were then determined by applying the normalization factor to the carefully measured reference cross section. The absorption spectrum of C_2H_5I-Cl was also measured at 300 Torr total pressure (N_2 bath gas) and 250 K using the same methods of producing radicals as for CH_3I-Cl. The reference wavelength used for the C_2H_5I-Cl spectral measurements was 365 nm.

All the absolute absorption cross section measurements at 350 nm for CH_3I-Cl and at 365 nm for C_2H_5I-Cl employed 308 nm photolysis of Cl_2 as the radical source. Typical concentrations employed in these measurements in units of 10^{13} molecules cm^{-3} were as follows: $[CH_3I] \approx 520$; $[Cl_2] \approx 58$–400; $[Cl]_0 \approx 0.53$–3.7 for the CH_3I-Cl experiments, and $[C_2H_5I] \approx 190$; $[Cl_2] \approx 130$–440; $[Cl]_0 \approx 1.4$–4.4 for the C_2H_5I-Cl experiments. High RI concentrations were employed to obtain ~99% conversion of Cl to RI−Cl at equilibrium (based on the equilibrium constants reported by Ayhens et al.[23] and Orlando et al.[30]). Each cross section measurement involved averaging 20 photolysis laser pulses. The CH_3I-Cl cross section at 350 nm, $\sigma(CH_3I)_{350}$ and the C_2H_5I-Cl cross section at 365 nm, $\sigma(C_2H_5I)_{365}$ were determined from the data using the following relationship:

$$\sigma(RI)_\lambda = X/(l[Cl]_0F) \quad (II)$$

In eq II, X is defined as in eq I (see above), l is the absorption path length (100 cm), $[Cl]_0$ is the concentration of chlorine atoms produced via laser flash photolysis of Cl_2, and F is the fraction of Cl atoms converted to adduct. As is typical for gas phase spectroscopic data, the absorbance is defined as $A = \ln(I_0/I_t)$ where I_0 is the transmitted light intensity before the laser fires and I_t is the transmitted light intensity at some time t after the laser fires; that is, A is a base e absorbance.

The parameter F in eq II can be evaluated using the following relationship:

$$F = (1 - F_1)(1 - F_2)(1 - F_3) \quad (III)$$

In eq III, F_1 is the fraction of Cl atoms that are lost by diffusion from the detection volume, reaction, or both with background impurities; F_2 is the fraction of Cl atoms that react with RI by H-abstraction rather than by addition; and F_3 is the fraction of RI−Cl ↔ Cl that exists as Cl when the two species are in equilibrium. Employing high concentrations of RI helps to keep F_1 and F_3 small, whereas employing relatively high total pressure minimizes F_2. On the basis of kinetic and thermodynamic data reported by Ayhens et al.[23] and Orlando et al.,[30] we estimate that $F_2 = 0.02$ and $F_3 = 0.005$ for CH_3I and $F_2 = 0.09$ and $F_3 = 0.001$ for C_2H_5I under the experimental conditions employed. The background loss rate of Cl atoms (typically found to be 50–100 s^{-1} in LFP studies of Cl kinetics that employ resonance fluorescence detection) is probably negligible as compared to the pseudo-first-order rate coefficient for Cl + RI, which is $(1.5$–$2.5) \times 10^5$ s^{-1} under the above experimental conditions. Hence, we conservatively assign F_1 a value of 0.01. The above considerations lead to the results $F = 0.96 \pm 0.02$ for CH_3I-Cl and $F = 0.89 \pm 0.07$ for C_2H_5I-Cl; the reported uncertainties are estimates of accuracy at the 95% confidence level.

Cross sections obtained from eq II were found to be independent of $[Cl]_0$ over the ranges specified above; that is, Beer's law was obeyed. Evaluation of $[Cl]_0$ required (i) careful measurements of $[Cl_2]$ and laser power; (ii) careful measurements of [RI], since both CH_3I and C_2H_5I absorb at 308 nm with cross sections in units of cm^2 $molecule^{-1}$ of 8.1×10^{-21} and 1.04×10^{-20}, respectively,[37] to generate concentrations of alkyl radicals that are a few percent of $[Cl]_0$; and (iii) careful measurements of the photolysis laser beam cross-sectional area and its divergence down the length of the cell (the laser beam area increased by a factor of 1.5 between the cell entrance and exit and was assumed to be the average of the entrance and exit areas for purposes of evaluating $[Cl]_0$).

The adduct spectra measured in this study at $T = 250$ K and $P = 300$ Torr N_2 are shown in Figure 3 and are given in digitized form in Table 1. The RI−Cl absorption spectra were measured on several days, verifying reproducibility of data, and were also measured by using two methods of radical generation, as discussed above. In the 350–500 nm spectral region, where measurements were performed using both methods of radical

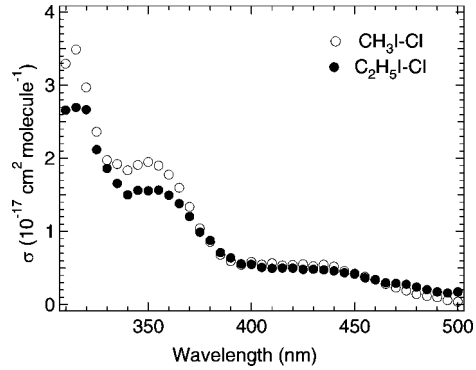

Figure 3. Absorption spectra of CH_3I-Cl (open circles) and C_2H_5I-Cl (filled circles) at a spectral resolution of 5.5 nm.

TABLE 1: Absorption Cross Sections for the RI−Cl Adducts as a Function of Wavelength at $T = 250$ K and a Spectral Resolution of 5.5 nm (FWHM)

λ^a	σ (CH_3I-Cl)^a	σ (C_2H_5I-Cl)^a	λ^a	σ (CH_3I-Cl)^a	σ (C_2H_5I-Cl)^a
310	3.29	2.66	410	0.57	0.50
315	3.49	2.69	415	0.54	0.50
320	2.97	2.66	420	0.54	0.50
325	2.36	2.12	425	0.55	0.48
330	1.97	1.86	430	0.52	0.48
335	1.92	1.66	435	0.54	0.47
340	1.84	1.50	440	0.52	0.46
345	1.91	1.56	445	0.46	0.43
350	1.95	1.56	450	0.42	0.42
355	1.90	1.56	455	0.38	0.37
360	1.78	1.49	460	0.34	0.34
365	1.60	1.38	465	0.28	0.30
370	1.33	1.20	470	0.23	0.29
375	1.04	0.99	475	0.19	0.28
380	0.86	0.88	480	0.14	0.24
385	0.68	0.71	485	0.12	0.20
390	0.59	0.64	490	0.10	0.17
395	0.54	0.56	495	0.06	0.16
400	0.58	0.55	500	0.04	0.17
405	0.55	0.51			

^{a} Units are λ (nm); σ (10^{-17} cm^2 molecule^{-1}).

production, the results obtained were essentially identical, again verifying data reproducibility. Consideration of uncertainties in the parameters that must be known to obtain the adduct cross section (see above) leads to an estimate of ±35% for the accuracy of the measured values for absolute absorption cross sections (95% confidence level). We report these cross sections in units of cm^2 molecule^{-1} (base e) to be $\sigma(CH_3I)_{350} = (1.95 \pm 0.68) \times 10^{-17}$ and $\sigma(C_2H_5I)_{365} = (1.35 \pm 0.47) \times 10^{-17}$.

The shape of the spectra reported in this study suggests that three different electronic states of RI−Cl are excited by photon absorption in the 310–500 nm wavelength range. Electronic excitation energies and oscillator strengths for CH_3I-Cl and C_2H_5I-Cl have been evaluated theoretically by Enami et al.[31] For both RI−Cl species, two strong absorption bands with similar oscillator strengths are predicted: one at $\lambda \sim 310$ nm and one at $\lambda \sim 340$ nm. Our spectra at $\lambda < 400$ nm are consistent with the theoretical results; however, we also observe evidence for a relatively weak transition at $\lambda \sim 420$ nm that is not predicted theoretically. The calculations do predict electronic transitions at $\lambda \sim 550$, 960, and 1080 nm that have little or no oscillator strength. Gravestock et al.[33] have recently reported observation of laser-induced fluorescence from CH_3I-Cl over the excitation wavelength range 345–375 nm. This interesting result establishes that at least one and possibly both of the electronic states excited by near-UV photons are bound.

The absorption cross sections reported in this study can be directly compared with those reported by Enami et al. at the fixed wavelengths 405, 435, and 488 nm[31] and over the range 440–500 nm.[32] Although the wavelength dependences of the cross sections agree reasonably well, the cross sections reported in this study are smaller than those reported by Enami et al. by about a factor of 4. Reasons for this difference are not readily ascertainable at this time. Since it does not appear that interfering transient absorbers were a problem in either study, an experimental problem, perhaps involving evaluation of the absolute concentration of radicals produced by the photolysis laser pulse, seems to be the most likely explanation for the discrepancy in reported cross sections.

Enami et al. attribute the absorption they observe at $\lambda > 405$ nm to the red tail of short wavelength transitions at ~310 and ~340 nm that they predict theoretically.[32] However, Gravestock et al.[33] point out that the Enami et al. interpretation of the CH_3I-Cl absorption at $\lambda > 405$ nm is almost certainly incorrect because (i) a 500 nm transition between two states with an energy separation of hc/λ with $\lambda = 340$ nm requires 9400 cm^{-1} of ground-state excitation where an infinitesimal Boltzmann population would be present and (ii) even if the adduct ground state were nonthermal, the required internal excitation would be significantly larger than the well-established CH_3I-Cl bond strength.[23,24,33] The above analysis further supports the existence of an electronic state at $\lambda > 400$ nm that is not predicted in the theoretical treatment of Enami et al.[32]

Radical–Radical Reaction Kinetics. When reaction mixtures containing only Cl_2, CH_3I, and N_2 are subjected to 308 nm laser flash photolysis and detectable levels of CH_3I-Cl are generated, we expect that CH_3I-Cl loss will be controlled by the following radical–radical reactions:

$$CH_3I-Cl + CH_3I-Cl \rightarrow 2\,CH_3I + Cl_2 \quad (9)$$

$$Cl + CH_3I-Cl \rightarrow CH_3I + Cl_2 \quad (10)$$

$$CH_3 + CH_3I-Cl \rightarrow CH_3I + CH_3Cl \quad (11)$$

$$CH_2I + CH_3I - Cl \rightarrow CH_2ICl + CH_3I \quad (12)$$

The products identified in reactions 9−12 above are the probable dominant products but not necessarily the only products that are energetically feasible. The Cl self-reaction is very slow and, therefore, is not listed above. If experimental conditions are adopted in which $T = 250$ K, $P = 300$ Torr N_2, $[Cl_2] = (1–3) \times 10^{15}$ molecules cm^{-3}, and $[CH_3I] > 1 \times 10^{15}$ molecules cm^{-3}, then Cl reacts rapidly with CH_3I to form ~98% CH_3I-Cl and ~2% CH_2I, [23] the equilibrium concentration ratio $[CH_3I-Cl]/[Cl]$ is >140,[23] and the concentration of CH_3 produced from CH_3I photolysis is typically only a few percent of the concentration of Cl produced from Cl_2 photolysis. Under such conditions, loss of CH_3I-Cl is expected to be controlled by reaction 9. Minor secondary production of Cl is expected via reactions 8 and 13, but the impact of these reactions on the derived value for k_9 is expected to be an insignificant source of uncertainty compared to the uncertainty in $[CH_3I-Cl]$.

$$CH_2I + Cl_2 \rightarrow CH_2ICl + Cl \quad (13)$$

Values for k_8 (250 K) and k_{13} (250 K) in units of 10^{-13} cm^3 molecule^{-1} s^{-1} are estimated on the basis of literature data at $T \geq 298$ K [40,41] to be 17 and 8, respectively.

To experimentally determine k_9 at $T = 250$ K and $P = 300$ Torr, experiments were carried out using (in units of 10^{15} molecules cm^{-3}) $[CH_3I] = (1.0–5.4)$ and $[Cl_2] = (1.0–3.5)$. Shown in Figure 4 is a typical CH_3I-Cl temporal profile observed at a monitoring wavelength of 380 nm. The data are

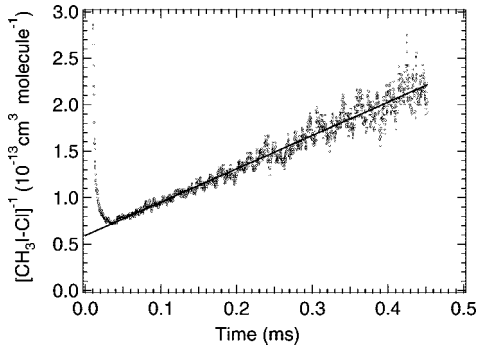

Figure 4. Typical RI−Cl absorbance temporal profile plotted as $[RI-Cl]^{-1}$ vs time. Experimental conditions: $T = 250$ K; $P = 300$ Torr N_2; R = CH_3; concentrations in units of 10^{15} molecules cm^{-3} = 5.43 CH_3I and 1.34 Cl_2. The solid line is obtained from a linear least-squares analysis; its slope gives $2k_9 = (3.44 \pm 0.02) \times 10^{-10}$ cm^3 $molecule^{-1}$ s^{-1} where the uncertainty is 2σ and represents precision only.

plotted as $[CH_3I-Cl]^{-1}$ vs time. The linearity of the plot is consistent with the hypothesis that adduct loss is dominated by reaction 9, and the self-reaction rate coefficient, $2k_9$, is obtained from the slope of the plot. Second-order rate coefficients obtained from several experiments over the ranges of $[Cl_2]$ and $[CH_3I]$ specified above, but at constant laser power, are in good agreement and give the following mean value for the self-reaction rate coefficient: $2k_9 = (3.49 \pm 0.24) \times 10^{-10}$ cm^3 $molecule^{-1}$ s^{-1}, where the uncertainty is 2σ and represents precision only. The accuracy of the derived value for $2k_9$ is limited by the accuracy of $[CH_3I-Cl]$, which in turn is limited by the accuracy of the CH_3I-Cl absorption cross section at the monitoring wavelength (380 nm); that is, ±35% (see above). Taking the CH_3I-Cl absorption cross section and imprecision to be the two main sources of uncertainty, we report $2k_9 = (3.5 \pm 1.2) \times 10^{-10}$ cm^3 $molecule^{-1}$ s^{-1}, where the uncertainty represents estimated accuracy at the 95% confidence level.

When reaction mixtures containing only Cl_2, C_2H_5I, and N_2 are subjected to 308 nm laser flash photolysis and detectable levels of C_2H_5I-Cl are generated, we expect that C_2H_5I-Cl loss will be controlled by the following radical–radical reactions:

$$C_2H_5I-Cl + C_2H_5I-Cl \rightarrow 2C_2H_5I + Cl_2 \quad (14)$$

$$Cl + C_2H_5I-Cl \rightarrow C_2H_5I + Cl_2 \quad (15)$$

$$C_2H_5 + C_2H_5I-Cl \rightarrow C_2H_5I + C_2H_5Cl \quad (16)$$

$$CH_3CHI + C_2H_5I-Cl \rightarrow CH_3CHICl + C_2H_5I \quad (17)$$

If experimental conditions are adopted in which $T = 250$ K, $P = 300$ Torr N_2, $[Cl_2] = (1-3) \times 10^{15}$ molecules cm^{-3}, and $[C_2H_5I] > 5 \times 10^{14}$ molecules cm^{-3}, then Cl reacts rapidly with C_2H_5I to form ∼90% C_2H_5I-Cl, ∼7% CH_3CHI and ∼3% CH_2CH_2I,[30] the equilibrium concentration ratio $[C_2H_5I-Cl]/[Cl]$ is >260,[30] and the concentration of C_2H_5 produced from C_2H_5I photolysis is very small compared to the concentration of Cl produced from Cl_2 photolysis. Under such conditions, loss of C_2H_5I-Cl is expected to be controlled predominantly by reaction 14. Minor secondary production of Cl is expected via reactions 18 and 19, but the impact of these reactions on the derived value for k_{14} is expected to be a small source of uncertainty compared to the uncertainty in $[C_2H_5I-Cl]$.

$$C_2H_5 + Cl_2 \rightarrow C_2H_5Cl + Cl \quad (18)$$

$$CH_3CHI + Cl_2 \rightarrow CH_3CHICl + Cl \quad (19)$$

On the basis of literature data at $T \geq 298$ K, $k_{18}(250\ K)$ is estimated to be 2.3×10^{-11} cm^3 $molecule^{-1}$ s^{-1}.[40] To our knowledge, no kinetic data for reaction 19 are reported in the literature. No Cl is regenerated from secondary chemistry involving the second H-transfer product, CH_2CH_2I, because this species rapidly decomposes to $I + C_2H_4$.[30]

To experimentally determine k_{14} at $T = 250$ K and $P = 300$ Torr, experiments were carried out using (in units of 10^{15} molecules cm^{-3}) $[C_2H_5I] = (0.64 - 2.17)$ and $[Cl_2] = (0.95 - 4.01)$. As was observed for loss of CH_3I-Cl (Figure 4), plots of $[C_2H_5I-Cl]^{-1}$ vs time were linear over 2–3 half-lives of decay; that is, second-order kinetics were obeyed. Values for k_{14} were obtained under the assumption that only reaction 14 contributes to the observed decay of absorbance; as discussed above, this assumption is likely to be pretty good, although small contributions from reactions 15–17 cannot be completely ruled out. Second-order rate coefficients were obtained from the slopes of the $[C_2H_5I-Cl]^{-1}$-vs-time plots for several experiments at constant laser power but over the ranges of $[Cl_2]$ and $[C_2H_5I]$ specified above. The results are quite reproducible and give the following mean value for the self-reaction rate coefficient: $2k_{14} = (3.97 \pm 0.40) \times 10^{-10}$ cm^3 $molecule^{-1}$ s^{-1}, where the uncertainty is 2σ and represents precision only. The accuracy of the derived value for $2k_{14}$ is limited by the accuracy of $[C_2H_5I-Cl]$, which in turn is limited by the accuracy of the C_2H_5I-Cl absorption cross section at the monitoring wavelength (365 or 380 nm), that is, ±35% (see above). Taking the C_2H_5I-Cl absorption cross section and imprecision to be the two main sources of uncertainty leads to the result $2k_{14} = (3.97 \pm 1.39) \times 10^{-10}$ cm^3 $molecule^{-1}$ s^{-1}. In this case, a small but nonnegligible additional uncertainty arises from the potential impacts of secondary chemistry on the derived value for k_{14}. Hence, we report the rate coefficient $2k_{14} = (4.0 \pm 1.6) \times 10^{-10}$ cm^3 $molecule^{-1}$ s^{-1}, where the uncertainty represents an estimate of accuracy at the 95% confidence level.

Kinetics of RI−Cl Reactions with O_2 and RI. To investigate the kinetics of the reaction of RI−Cl with O_2, RI−Cl absorbance temporal profiles were measured in 300 Torr of O_2 with experimental conditions adjusted to high [RI] and low $[Cl]_0$ to minimize the contribution of radical–radical reactions to RI−Cl removal.

$$CH_3I-Cl + O_2 \rightarrow \text{products} \quad (20)$$

$$C_2H_5I-Cl + O_2 \rightarrow \text{products} \quad (21)$$

Little or no reaction of RI−Cl with O_2 was observed at $T \sim 250$ K. To establish upper limits for k_{20} and k_{21}, back-to-back experiments were carried out in which experimental conditions were held constant except that N_2 and O_2 were interchanged as the bath gas. Plots of ln A vs time for one set of back-to-back experiments aimed at evaluating k_{20} are shown in Figure 5. Plots of ln A vs time are nonlinear in both N_2 and O_2 in a manner that suggests the dominance of radical–radical reactions controlling CH_3I-Cl removal, particularly at short times after the laser flash when the adduct concentration is relatively high. Linear least-squares analyses of the CH_3I-Cl temporal profiles at 2 – 4.5 ms after the laser flash (Figure 5) give pseudo-first-order decay rates (k_d) of 413 ± 17 s^{-1} in 300 Torr N_2 and 420 ± 17 s^{-1} in 300 Torr O_2 (uncertainties are 2σ, precision only). Data analysis was restricted to times less than 4.5 ms after the laser flash because there was so little absorption at later times that quantitative kinetic analysis was precluded. Reactions 9–12, diffusion of RI−Cl out of the detection volume, and reaction of RI−Cl with background impurities in the bath gases may all contribute to the time evolution of absorbance for the data shown in Figure 5. However, temporal profiles observed in 300 Torr O_2 were indistinguishable from those observed in 300 Torr N_2

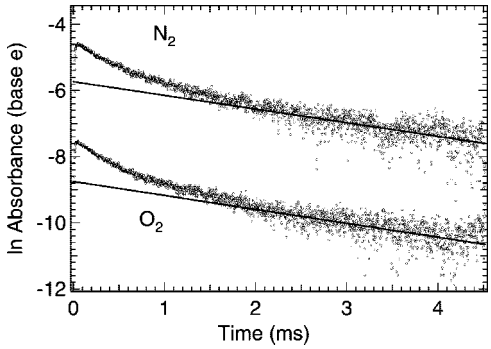

Figure 5. Comparison of CH_3I absorbance temporal profiles observed at $T = 250$ K and $P = 300$ Torr in N_2 vs O_2 bath gas. The CH_3I concentration was 4.4×10^{15} molecules cm^{-3} in both experiments. Best fit slopes are 413 ± 17 and 420 ± 17 s^{-1} for the data obtained in N_2 and O_2, respectively, within the time intervals 2.0–4.5 ms after the laser flash (uncertainties are 2σ and represent precision only). For the sake of clarity, the data obtained in O_2 have been offset downward by 3 units of ln concentration.

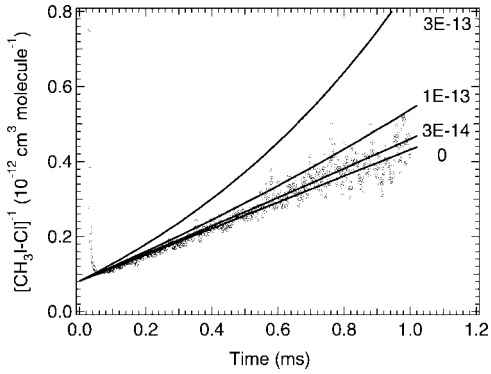

Figure 6. CH_3I-Cl absorbance temporal profile plotted as $[CH_3I-Cl]^{-1}$ vs time. Experimental conditions: $T = 250$ K; $P = 300$ Torr N_2; concentrations in units of 10^{14} molecules $cm^{-3} = 36.6$ $[CH_3I]$, 9.81 $[Cl_2]$, and ~0.10 $[Cl]_0$. The straight line represents simulation of the $[CH_3I-Cl]^{-1}$-vs-time plot expected for $2k_9 = 3.5 \times 10^{-10}$ cm^3 molecule^{-1} s^{-1} and $k_3 = 0$. The curved lines are simulations of the $[CH_3I-Cl]^{-1}$ vs time plots expected if k_3 had the values shown in the figure (in units of cm^3 molecule^{-1} s^{-1}).

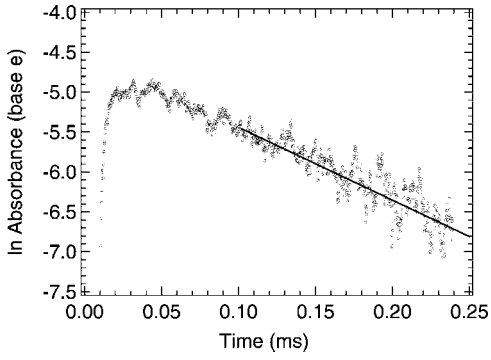

Figure 7. Typical absorbance temporal profile observed following 308 nm laser flash photolysis of $Cl_2/RI/NO_x/N_2$ mixtures at $T = 250$ K and $P = 300$ Torr. The data shown were obtained with $NO_x = NO$ and $R = CH_3$. Concentrations in units of 10^{14} molecules cm^{-3} are $[CH_3I] = 56.2$, $[NO] = 3.92$, $[Cl_2] = 5.19$, and $[Cl]_o \approx 0.05$. The solid line is obtained from a linear least-squares analysis of the ln absorbance vs time (t) data at $t > 100$ μs after the laser flash; its slope gives the pseudo-first-order decay rate 9020 s^{-1}.

bath gas. Similar behavior was observed in analogous experiments in which C_2H_5I-Cl temporal profiles were monitored.

To put reasonable upper limits on k_{20} and k_{21}, it is necessary to consider the fact that secondary chemistry is not identical in

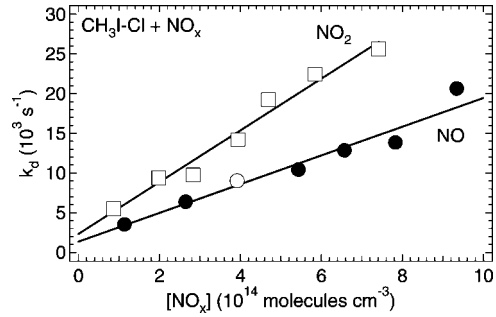

Figure 8. Plots of pseudo-first-order CH_3I-Cl decay rates (k_d) versus $[NO_x]$ for data obtained at $T = 250$ K and $P = 300$ Torr N_2. The solid lines are obtained from linear least-squares analyses; their slopes give the following rate coefficients in units of 10^{-11} cm^3 molecule^{-1} s^{-1} (uncertainties are 2σ and represent precision only): $k_{22} = 1.81 \pm 0.28$ and $k_{24} = 3.26 \pm 0.48$. The open data point is the one obtained from the data shown in Figure 7.

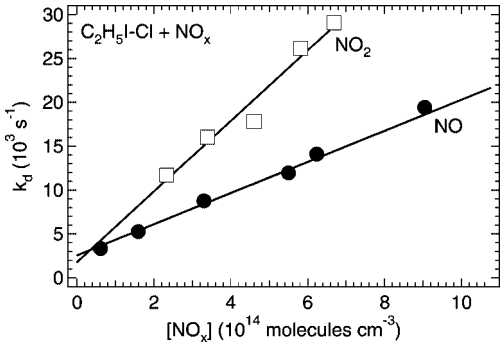

Figure 9. Plots of pseudo-first-order C_2H_5I-Cl decay rates (k_d) versus $[NO_x]$ for data obtained at $T = 256$ K and $P = 300$ Torr N_2. The solid lines are obtained from linear least-squares analyses; their slopes give the following rate coefficients in units of 10^{-11} cm^3 molecule^{-1} s^{-1} (uncertainties are 2σ and represent precision only): $k_{23} = 1.78 \pm 0.14$ and $k_{25} = 4.02 \pm 0.93$.

N_2 and O_2 bath gases. In O_2, the H-abstraction products CH_2I and CH_3CHI, as well as the alkyl radicals CH_3 and C_2H_5 (produced from 308 nm photolysis of CH_3I and C_2H_5I, respectively) react with O_2 to produce species that are less reactive than their radical precursors. The alkyl radicals CH_3 and C_2H_5 are converted to peroxy radicals. It is reported in the literature that the dominant channel for the reaction of CH_2I with O_2 is production of IO + H_2CO,[42] although recent (currently unpublished) results bring this conclusion into question.[43] At present, there appears to be insufficient information to establish yields of CH_3CHIOO and IO + CH_3CHO from the $CH_3CHI + O_2$ reaction.[30] It is possible (though unlikely) that in the presence of O_2, some reduction in the rates of loss of CH_3I-Cl via reactions 10–12 and C_2H_5I-Cl via reactions 15–17 is compensated for by very slow but nonzero rates of reaction of $RI-Cl$ with O_2. Taking this potential complication into account, the results of 12 back-to-back experiments like the ones shown in Figure 5 for CH_3I-Cl and 25 analogous back-to-back experiments for C_2H_5I-Cl lead to the following conservative upper limits for k_{20} and k_{21} at $P = 300$ Torr and $T = 250$ K in units of 10^{-17} cm^3 molecule^{-1} s^{-1}: $k_{20} < 1.0$ and $k_{21} < 2.5$.

Product studies conducted by Bilde and Wallington[27] and by Orlando et al.[30] provide evidence for the occurrence of reactions 3 and 5. Orlando et al.[30] have modeled the kinetics in the two experiments[27,30] on the basis of reasonable assumed reaction mechanisms and obtain the estimates $k_3(298\ K) = (5-10) \times 10^{-13}$ cm^3 molecule^{-1} s^{-1} and $k_5(298\ K) = (2-5) \times 10^{-13}$ cm^3 molecule^{-1} s^{-1}.

We were unable to observe strong evidence for the occurrence of RI + RI−Cl reactions, but our data do allow upper limits for k_3 and k_5 at 250 K to be deduced. Our approach involves kinetic simulations of the data in N_2 bath gas that were employed to evaluate RI + O_2 rate coefficients; as mentioned above, these data were obtained under experimental conditions in which radical concentrations were lower than in the experiments aimed at investigating radical–radical reaction kinetics. The simulations employ simple two-reaction schemes: reactions 3 and 9 for the methyl iodide data and reactions 5 and 14 for the ethyl iodide data. A typical result for the methyl iodide case is shown in Figure 6, where the data are plotted as $[CH_3I-Cl]^{-1}$ vs time. Even at the relatively low radical concentrations employed to obtain the data in Figure 6, the data are well-simulated, assuming the value for $2k_9$ obtained as described above and assuming that $k_3 = 0$. The simulations suggest that upward curvature in the $[CH_3I-Cl]^{-1}$-vs-time plot would be readily observable if $k_3 \geq 3 \times 10^{-13}$ cm^3 molecule^{-1} s^{-1}, so we adopt this value as a conservative upper limit. A similar analysis of the ethyl iodide data suggests that $k_5 \leq 5 \times 10^{-13}$ cm^3 molecule^{-1} s^{-1}. Direct comparison of our results with literature values is hampered by the fact that our data were obtained at 250 K, whereas most previous results[27,30] were obtained at 298 K. At 250 K, the upper limit value for k_3 obtained in this study is lower than the suggested range of values for k_3 at 298 K that are consistent with Orlando et al.'s[30] analysis of the results of Bilde and Wallington.[27] In their studies at 216 and 296 K using LIF detection of CH_3I-Cl (this issue), Gravestock et al.[33] conclude that CH_3I-Cl decay can be completely attributed to radical–radical reactions,; that is, in agreement with our findings, they obtain no compelling evidence for the occurrence of the $CH_3I-Cl + CH_3I$ reaction.

Kinetics of RI−Cl Reactions with NO and NO_2. The reactions of RI−Cl with NO and NO_2 were studied at $T = 250$ K and $P = 300$ Torr (N_2 bath gas) under pseudo-first-order conditions with $[NO_x] >> [RI-Cl]$.

$$CH_3I-Cl + NO \rightarrow \text{products} \quad (22)$$

$$C_2H_5I-Cl + NO \rightarrow \text{products} \quad (23)$$

$$CH_3I-Cl + NO_2 \rightarrow \text{products} \quad (24)$$

$$C_2H_5I-Cl + NO_2 \rightarrow \text{products} \quad (25)$$

The reagent concentrations (units are 10^{14} molecules cm^{-3}) used in experiments investigating reactions 22 and 24 were as follows: $[Cl_2]$ = (5.4–10.0); $[Cl]_0$ = (0.05–0.07); $[CH_3I]$ = (48–56); [NO] = (1.13–11.0); $[NO_2]$ = (0.866–7.42). For studies of reactions 23 and 25, the following concentrations were employed (units are 10^{14} molecules cm^{-3}): $[Cl_2]$ = (9.0–10.1); $[Cl]_0$ = (0.08–0.28); $[C_2H_5I]$ = (15–16); [NO] = (0.612–10.8); $[NO_2]$ = (2.33–6.69). Relatively low radical concentrations were employed to minimize the effect of radical–radical side reactions on the observed absorbance temporal profiles. Experimental conditions of high [RI] (>10^{15} molecules cm^{-3}) and low temperature (250 K) minimized the contribution of Cl reactions with NO and NO_2 to observed RI−Cl kinetics by driving the RI−Cl ↔ Cl equilibria to over 99% adduct.[23,30]

$$Cl + NO + M \rightarrow ClNO + M \quad (26)$$

$$Cl + NO_2 + M \rightarrow ClNO_2 + M \quad (27a)$$

$$\rightarrow ClONO + M \quad (27b)$$

As typified by the data shown in Figure 7, absorbance decays were exponential; that is, plots of ln A vs time were linear, as would be expected under the experimental conditions employed (see above). Measured pseudo-first-order decay rates (k_d), obtained from the slopes of plots such as the one shown in Figure 7) are plotted as a function of [RI] in Figures 8 and 9. The slopes of the k_d-vs-[RI] plots give the following second-order rate coefficients in units of 10^{-11} cm^3 molecule^{-1} s^{-1} (uncertainties are 2σ and represent precision only): $k_{22} = 1.81 \pm 0.28$, $k_{24} = 3.26 \pm 0.48$, $k_{23} = 1.78 \pm 0.14$, and $k_{25} = 4.02 \pm 0.93$. For $[Cl]_0 \sim 1 \times 10^{13}$ per cm^3 (see above), reactions 9 and 14 make small but significant contributions to RI−Cl adduct removal. As a result, pseudo-first-order decay rates were obtained from the slopes of plots such as the one shown in Figure 7 using only data obtained at times when A < 0.004 (i.e., $[RI-Cl] < 2 \times 10^{12}$ molecules cm^{-3}). On the basis of the above discussion of radical–radical reaction kinetics, we consider the contribution of reactions 9 and 14 insignificant when $[RI-Cl] < 2 \times 10^{12}$ molecules cm^{-3}. Since side reactions have little or no impact on the accuracy of the reported rate coefficients, it appears that accuracy is limited by precision and by the accuracy with which the concentrations of NO and NO_2 were known (estimated to be ±5% for each). Hence, we report the following rate coefficients in units of 10^{-11} cm^3 molecule^{-1} s^{-1}: $k_{22} = 1.8 \pm 0.4$, $k_{24} = 3.3 \pm 0.6$, $k_{23} = 1.8 \pm 0.3$, and $k_{25} = 4.0 \pm 0.9$; the uncertainties are estimates of accuracy at the 95% confidence level.

Although there are no other reported measurements of k_{22}–k_{25} with which to compare our results, it is of interest to note that the rate coefficients reported in this study are very similar in magnitude to rate coefficients for the reactions of $(CH_3)_2S-Cl$,[34] SCS-Cl,[35] and $CH_3(O)S(Cl)CH_3$[36] with NO and NO_2, all of which were measured using a technique that is analogous to the one employed in this study. All $X-Cl + NO_x$ (X = $(CH_3)_2S$, SCS, $(CH_3)_2SO$, CH_3I, C_2H_5I) rate coefficients are within the range (1–4) × 10^{-11} cm^3 molecule^{-1} s^{-1}, and reactivity of these adducts with O_2 is not observed. It appears that Cl adducts react rapidly with compounds such as NO and NO_2, in which transfer of the chlorine atom to generate ClNO, $ClNO_2$, or ClONO is energetically favorable. Because Cl−OO is bound by only 19 kJ mol^{-1},[44] the chlorine transfer reaction between the above-mentioned adducts and O_2 cannot occur at a significant rate at $T < 300$ K.

Acknowledgment. This research was supported by the NSF Atmospheric Chemistry Program (Grant ATM-0350185) and the NASA Upper Atmosphere Research Program (Grant NNG06GD90G).

References and Notes

(1) Liss, P. S.; Slater, P. G. *Nature* **1974**, *247*, 181.
(2) Rasmussen, R. A.; Khalil, M. A. K.; Gunawardena, R.; Hoyt, S. D. *J. Geophys. Res.* **1982**, *87*, 3086.
(3) Singh, H. B.; Salas, L. J.; Stiles, R. E. *J. Geophys. Res.* **1983**, *88*, 3684.
(4) Reifenhauser, W.; Heumann, K. G. *Atmos. Environ. A* **1992**, *26*, 2905.
(5) Oram, D. E.; Penkett, S. A. *Atmos. Environ.* **1994**, *28*, 1159.
(6) Davis, D.; Crawford, J.; Liu, S.; McKeen, S.; Bandy, A.; Thornton, D.; Rowland, F.; Blake, D. *J. Geophys. Res.* **1996**, *101*, 2135.
(7) Moore, R. M.; Tokarczyk, R. *Geophys. Res. Lett.* **1992**, *19*, 1779.
(8) Carpenter, L. J.; Sturges, W. T.; Penkett, S. A.; Liss, P. S.; Alicke, B.; Hebestreit, K.; Platt, U. *J. Geophys. Res.* **1999**, *104*, 1679.
(9) Klick, S.; Abrahamsson, K. *J. Geophys. Res.* **1992**, *97*, 12683.
(10) Yokouchi, Y.; Mukai, H.; Yamamoto, H.; Otsuki, A.; Saitoh, C.; Nojiri, Y. *J. Geophys. Res.* **1997**, *102*, 8805.
(11) Schall, C.; Heumann, K. G. *Fresenius' J. Anal. Chem.* **1993**, *346*, 717.
(12) Happell, J. D.; Wallace, D. W. R. *Geophys. Res. Lett.* **1996**, *23*, 2105.
(13) Chameides, W. L.; Davis, D. D. *J. Geophys. Res.* **1980**, *85*, 7383.

(14) Vogt, R.; Sander, R.; Von Glasow, R.; Crutzen, P. J. *J. Atmos. Chem.* **1999**, *32*, 375.
(15) McFiggans, G.; Plane, J. M. C.; Allan, B. J.; Carpenter, L. J.; Coe, H.; O'Dowd, C. *J. Geophys. Res.* **2000**, *105*, 14371.
(16) Cronkhite, J. M.; Stickel, R. E.; Nicovich, J. M.; Wine, P. H. *J. Phys. Chem. A* **1999**, *103*, 3228.
(17) Jimenez, J. L.; Bahreini, R.; Cocker, D. R.; Zhuang, H.; Varutbangkul, V.; Flagan, R. C.; Seinfeld, J. H.; O'Dowd, C. D.; Hoffmann, T. *J. Geophys. Res.* **2003**, *108*, 25.
(18) Burkholder, J. B.; Curtius, J.; Ravishankara, A. R.; Lovejoy, E. R. *Atmos. Chem. Phys.* **2004**, *4*, 19.
(19) McFiggans, G.; Coe, H.; Burgess, R.; Allan, J.; Cubison, M.; Alfarra, M. R.; Saunders, R.; Saiz-Lopez, A.; Plane, J. M. C.; Wevill, D. J.; Carpenter, L. J.; Rickard, A. R.; Monks, P. S. *Atmos. Chem. Phys.* **2004**, *4*, 701.
(20) Solomon, S.; Garcia, R. R.; Ravishankara, A. R. *J. Geophys. Res.* **1994**, *99*, 20491.
(21) Hoffmann, S. M. A.; Smith, D. J.; Urena, A. G.; Steele, T. A.; Grice, R. *Mol. Phys.* **1984**, *53*, 1067.
(22) Hoffmann, S. M. A.; Smith, D. J.; Urena, A. G.; Grice, R. *Chem. Phys. Lett.* **1984**, *107*, 99.
(23) Ayhens, Y. V.; Nicovich, J. M.; McKee, M. L.; Wine, P. H. *J. Phys. Chem. A* **1997**, *101*, 9382.
(24) Lazarou, Y. G.; Kambanis, K. G.; Papagiannakopoulos, P. *Chem. Phys. Lett.* **1997**, *271*, 280.
(25) Kambanis, K. G.; Lazarou, Y. G.; Papagiannakopoulos, P. *Chem. Phys. Lett.* **1997**, *268*, 498.
(26) Goliff, W. S.; Rowland, F. S. *Geophys. Res. Lett.* **1997**, *24*, 3029.
(27) Bilde, M.; Wallington, T. J. *J. Phys. Chem. A* **1998**, *102*, 1550.
(28) Cotter, E. S. N.; Booth, N. J.; Canosa-Mas, C. E.; Gray, D. J.; Shallcross, D. E.; Wayne, R. P. *Phys. Chem. Chem. Phys.* **2001**, *3*, 402.
(29) Cotter, E. S. N.; Booth, N. J.; Canosa-Mas, C. E.; Wayne, R. P. *Atmos. Environ.* **2001**, *35*, 2169.
(30) Orlando, J. J.; Piety, C. A.; Nicovich, J. M.; McKee, M. L.; Wine, P. H. *J. Phys. Chem. A* **2005**, *109*, 6659.
(31) Enami, S.; Hashimoto, S.; Kawasaki, M.; Nakano, Y.; Ishiwata, T.; Tonokura, K.; Wallington, T. J. *J. Phys. Chem. A* **2005**, *109*, 1587.
(32) Enami, S.; Yamanaka, T.; Hashimoto, S.; Kawasaki, M.; Tonokura, K. *J. Phys. Chem. A* **2005**, *109*, 6066.
(33) Gravestock, T. J.; Blitz, M. A.; Heard, D. E. *J. Phys. Chem. A* **2008**, *112*, xxxx.
(34) Urbanski, S. P.; Wine, P. H. *J. Phys. Chem. A* **1999**, *103*, 10935.
(35) Dookwah-Roberts, V.; Soller, R.; Nicovich, J. M.; Wine, P. H. *J. Photochem. Photobiol., A* **2005**, *176*, 114.
(36) Kleissas, K. M.; Nicovich, J. M.; Wine, P. H. *J. Photochem. Photobiol., A* **2007**, *187*, 1.
(37) Sander, S. P.; Finlayson-Pitts., B. J.; Friedl, R. R.; Golden, D. M.; Huie, R. E.; Keller-Rudek, H.; Kolb, C. E.; Kurylo, M. J.; Molina, M. J.; Moortgat, G. K.; Orkin, V. L.; Ravishankara, A. R.; Wine, P. H. Chemical Kinetics and Photochemical Data for Use in Atmospheric Studies, JPL Publication 06-2, Jet Propulsion Laboratory: Pasadena, CA, 2006.
(38) Estupinan, E. G.; Nicovich, J. M.; Wine, P. H. *J. Phys. Chem. A* **2001**, *105*, 9697.
(39) See, for example, Atkins, P.; de Paula, J. *Physical Chemistry*, 8th ed., W.H. Freeman & Co.: New York, 2006, p. 811.
(40) Timonen, R. S.; Gutman, D. *J. Phys. Chem.* **1986**, *90*, 2987.
(41) Seetula, J. A.; Gutman, D.; Lightfoot, P. D.; Rayes, M. T.; Senkan, S. M. *J. Phys. Chem.* **1991**, *95*, 10688.
(42) Enami, S.; Ueda, J.; Goto, M.; Nakano, Y.; Aloisio, S.; Hashimoto, S.; Kawasaki, M. *J. Phys. Chem. A* **2004**, *108*, 6347.
(43) Gravestock, T. J.;Thesis, University of Leeds, UK, 2006.
(44) Nicovich, J. M.; Kreutter, K. D.; Shackelford, C. J.; Wine, P. H. *Chem. Phys. Lett.* **1990**, *179*, 367.

JP800270R